High-Temperature Phase Equilibria of Duplex Stainless Steels Assessed with a Novel *In-Situ* Neutron Scattering Approach

NIKLAS PETTERSSON, STEN WESSMAN, STAFFAN HERTZMAN, and ANDREW STUDER

Duplex stainless steels are designed to solidify with ferrite as the parent phase, with subsequent austenite formation occurring in the solid state, implying that, thermodynamically, a fully ferritic range should exist at high temperatures. However, computational thermodynamic tools appear currently to overestimate the austenite stability of these systems, and contradictory data exist in the literature. In the present work, the high-temperature phase equilibria of four commercial duplex stainless steel grades, denoted 2304, 2101, 2507, and 3207, with varying alloying levels were assessed by measurements of the austenite-to-ferrite transformation at temperatures approaching 1673 K (1400 °C) using a novel *in-situ* neutron scattering approach. All grades became fully ferritic at some point during progressive heating. Higher austenite dissolution temperatures were measured for the higher alloyed grades, and for 3207, the temperature range for a single-phase ferritic structure approached zero. The influence of temperatures in the region of austenite dissolution was further evaluated by microstructural characterization using electron backscattered diffraction of isothermally heat-treated and quenched samples. The new experimental data are compared to thermodynamic calculations, and the precision of databases is discussed.

DOI: 10.1007/s11661-016-3953-1

I. INTRODUCTION

DUPLEX stainless steels are commercially important materials due to their excellent corrosion resistance in combination with high mechanical strength.[1] The microstructure consists of roughly equal amounts of ferrite (α) and austenite (γ) phases. The success of this category of alloys is primarily due to the increased use of nitrogen as an alloying element.[2] Nitrogen is a strong austenite stabilizer and has beneficial effects on corrosion resistance, mechanical properties, and weldability. The effect on mechanical properties is mainly due to the increased strength[3] and work hardening[4] of the austenite phase in which most of the nitrogen is located. Nitrogen also enhances the pitting corrosion resistance of the austenite phase in chloride containing environments,[5,6] especially in the presence of Mo.[5] The resistance to localized corrosion is primarily determined by the levels of Cr, Mo, and N, as described by the empirical pitting resistance equivalent formula PREN = pct Cr + 3.3 × pct Mo + 16 × pct N.[7] The influence on weldability is due to the strong austenite forming effect in combination with rapid diffusion of nitrogen, which promotes effective austenite formation in the heat-affected zone (HAZ) during subsequent cooling.[8,9] Due to the strong influence of alloying content on the properties, there is a wide range of duplex grades available, ranging from lower alloyed lean duplex grades, typically designed for structural applications (*e.g.*, storage tanks, bridges, and water heaters), to higher alloyed super and hyper duplex grades for use in severely corrosive environments (*e.g.*, seawater).

In terms of materials design, the alloying is balanced to obtain an equilibrated microstructure with the desired ratio of ferrite and austenite and with similar corrosion resistance (*e.g.*, PREN) in both phases after solution annealing. The thermodynamic basis for this category of steels is the Fe-Cr-Ni-N-system, where Ni are N are austenite stabilizing, while Cr is a ferrite stabilizing element. The influence of other alloying elements can be expressed in terms of Ni or Cr equivalents, where Mo belongs to the ferrite stabilizing group while N and C are austenite stabilizing.[10] The duplex steels are designed to solidify in the single-phase ferritic mode with formation of austenite by precipitation in the solid state.[1] The high-temperature phase equilibria should thus show an interval below solidus where the material is fully ferritic, and upon reheating, it should be possible to obtain a single-phase ferritic microstructure. The high-temperature equilibria, hence, are important from a materials design and manufacturing perceptive and also from a fabrication perspective, since the material will be exposed to high temperature during welding.

NIKLAS PETTERSSON and STEN WESSMAN are with Swerea KIMAB AB, P.O. Box 7047, 164 07 Kista, Sweden. Contact e-mail: niklas.pettersson@swerea.se STAFFAN HERTZMAN is with Outokumpu Stainless Research Foundation, Brinellvgen 23, 100 44, Stockholm, Sweden. ANDREW STUDER is with the Australian Nuclear Science and Technology Organisation, Locked Bag 2001, Kirrawee DC, NSW 2232, Australia.

Manuscript submitted October 7, 2016.
Article published online January 20, 2017

However, experimental evidence for this ferritic single-phase region is conflicting and the CALPHAD-based computational thermodynamic tools appear to overestimate the austenite stability. In a work by Hertzman *et al.*,[8] three commercial grade duplex stainless steels were subjected to welding simulation and the temperature to ferritize the materials was experimentally determined to 1613 K to 1618 K (1340 °C to 1345 °C), 1618 K to 1623 K (1345 °C to 1350 °C), and 1653 K to 1658 K (1380 °C to 1385 °C) for 2304, 2205, and 2507, respectively. The evaluation was based on optical microscopy and the material was considered as completely ferritized when the heat-treated and quenched microstructure consisted of equiaxed ferrite with allotriomorphic and Widmanstätten austenite. In contrast, Ramirez *et al.*[11] reported that in attempts to ferritize five duplex stainless steels, only the lowest alloyed 2304 could be ferritized, while, *e.g.*, 2205 and 2507 still contained signs of undissolved austenite after heat treatment at 1658 K (1385 °C) and, consequently, were considered to lack a ferritic region. Thermodynamic calculations were presented as secondary evidence, confirming that only 2304 out of the five investigated alloys had a ferritic single-phase region.

Possible contributory explanations for this confused situation are that extensive austenite formation inevitably occurs in the solid state during cooling, even if a fast cooling rate is used, and also that the volatility of the very important alloying element nitrogen makes it difficult to perform reliable and reproducible experiments at these very high temperatures. The question of the fully ferritic condition of duplex stainless steels is closely related to the solubility of nitrogen in these steels, and small changes in the nitrogen content have a considerable effect on the phase equilibria.[8] Therefore, it is of significant importance that nitrogen losses or uptakes in the experiments are avoided. The available experimental assessments also rely on postexperimental metallographic investigations, which are open to different interpretations.

The use of *in-situ* methods such as synchrotron high-energy X-ray diffraction or neutron scattering should be able to provide unique insight into the high-temperature equilibria of these steels. In previous work by Palmer *et al.*,[12] *in-situ* synchrotron high-energy X-ray diffraction was applied to observe phase transformation during spot welding of the duplex grade 2205. It was reported that a completely ferritic structure was obtained in parts of the HAZ at 1615 K (1342 °C) for that particular alloy.

The purpose of the present study is to examine the high-temperature phase equilibria in four commercial duplex steels, ranging from lower alloyed lean duplex grades to higher alloyed super and hyper duplex grades, using *in-situ* neutron scattering. The advantage with neutrons compared to high-energy X-rays is the larger analysis depth as a result of scattering being a nucleus event rather than an electron cloud interaction. This provides a unique possibility for *in-situ* bulk analysis, which makes the analysis less sensitive to possible nitrogen losses in the surface region during the experiment. One alternative could be to use a nitrogen-containing shielding gas. However, this introduces the risk for a nitrogen uptake instead, which would influence the austenite stability in the other direction. Measurements of the austenite high-temperature stability using *in-situ* neutron diffraction can provide reliable information about the high-temperature equilibria that is currently missing for this important class of steel. Isothermal heat treatments have also been performed, and the resulting microstructures after quenching have been analyzed by electron backscattered diffraction (EBSD). The experimental results are compared with thermodynamic calculations, and the precision of the databases is discussed.

II. EXPERIMENTAL DETAILS

A. *Materials*

Four commercial duplex stainless steel grades were included in this investigation. The lean duplex grades 2304 and LDX 2101* and the super duplex 2507 were supplied by Outokumpu Stainless AB in the form of 6-mm-thick plate. The hyper duplex SAF 3207 HD** was supplied by AB Sandvik Materials Technology as seamless tube with 6.35-mm wall thickness. The chemical compositions of the different steel grades are given in Table I.

*LDX 2101 is a trademark of Outokumpu Stainless AB.

**SAF 3207 HD is a trademark of AB Sandvik Materials Technology.

B. *In-Situ Neutron Scattering*

Neutron diffraction was performed at the Bragg Institute of the Australian Nuclear Science and Technology Organisation using the high-intensity powder diffractometer WOMBAT[13] located on the TG1 thermal guide at the OPAL reactor at Lucas Heights. The instrument was used in symmetric Bragg geometry, and a vertically focusing Ge (115) monochromator was used to produce a monochromated incident beam with a neutron wavelength of 1.53 Å. The detection system comprises a radial oscillating collimator (to remove any unwanted Bragg peaks from, in this case, the furnace) and a monolithic curved area detector covering a continuous 2θ range of 120 deg by 200 mm in height.

The *in-situ* experiments were performed using an ILL-type high-temperature vacuum furnace in which the samples were held in argon atmosphere using a corundum crucible sample holder. The furnace temperature was controlled by a thermocouple, which was positioned near the sample within the sample holder. Cylindrical specimens, Ø5 × 40 mm, were initially heated to 1473 K (1200 °C) at a rate of 50 K/s. From 1473 K (1200 °C), the temperature was then progressively raised by 4 K/min to a maximum of 1703 K (1430 °C), depending on

Table I. Chemical Composition of the Different Duplex Stainless Steel Grades in Weight Percent with Fe Content as Balance, Measured with Combined X-Ray Fluorescence and Combustion Analysis

Designation	Standard	C	Si	Mn	P	S	Cr	Ni	Mo	Cu	N
2304	UNS32304	0.022	0.41	1.36	0.025	0.001	23.29	4.85	0.34	0.24	0.12
2101	UNS32101	0.021	0.66	4.86	0.021	0	21.27	1.64	0.20	0.24	0.21
2507	UNS32750	0.012	0.30	0.83	0.023	0.001	24.84	6.90	3.80	0.18	0.28
3207	UNS33207	0.014	0.25	0.82	—	—	31.38	7.07	3.5	0.21	0.48

the alloy, and then ramped down by 4 K/min to also capture the transformations on cooling. The 2304 and 2101 were heated to 1648 K (1375 °C) and the 2507 and 3207 to 1507 K (1430 °C). The beam width was approximately 10 mm, and the height was matched to the sample length (40 mm). The diffraction patterns were acquired with a 10-second acquisition time during the full run. The diffraction data were postprocessed by azimuthal integration, and pseudo-Voigt profiles were then applied to determine the peak area intensities of the ferrite and austenite peaks as a function of temperature.

C. *Isothermal Heat Treatments*

Isothermal heat treatments were done on a 40 × 20-mm sized specimen (in the shape of strips) in a laboratory furnace under atmospheric conditions at temperatures between 1593 K and 1673 K (1320 °C and 1400 °C) for 0.5 hours followed by quenching in brine. A thermocouple was placed within the furnace close to the sample.

D. *Electron Microscopy*

The isothermally heat-treated specimens were evaluated using EBSD to map the distribution of the austenite and ferrite phases. The plate material (2304, 2101, and 2507) was sectioned parallel to the rolling direction, while the tube material (3207) was sectioned parallel to the extrusion direction, to reveal any residual banded austenite structure. The samples for EBSD were prepared down to 1-μm diamond suspension finish, and then they were polished in acetic alumina suspension for 10 minutes followed by polishing in colloidal silica solution in a vibratory polisher for a minimum of 2 hours. The EBSD analysis was performed at 15-kV acceleration voltage using a JEOL[†] 7001F field-emission gun scanning electron microscope equipped with a NordlysNano EBSD detector (Oxford Instruments, Oxford, United Kingdom). The EBSD postprocessing was done using the Channel 5 software package.

[†]JEOL is a trademark of JEOL Ltd., Tokyo.

III. RESULTS AND DISCUSSION

A. *Thermodynamic Calculations*

Figure 1 shows isopleth sections for 2304, 2101, 2507, and 3207 calculated with the Thermo-Calc software[14] using the TCFE7 steels/Fe-alloys database version 7.[15] The calculations were performed for the compositions listed in Table I (omitting sulfur and phosphorus). The only grade that clearly displays a single-phase ferritic region is the lowest alloyed 2304. The 2101 is on the limit to the $\alpha + \gamma + L$ equilibria. The higher alloyed 2507 and 3207 both have compositions that will pass the three-phase field during solidification and are, thus, never fully ferritic according to the calculations.

B. *In-Situ Measurements of the High-Temperature Phase Equilibria*

The neutron diffraction patterns at ambient temperature of the four investigated grades are shown in Figure 2. The patterns consist of peaks of ferrite (body-centered cubic) and austenite (face-centered cubic) mixed with peaks from the Al_2O_3 sample holder (trigonal $R\bar{3}c$). The austenite {111} and ferrite {110} both overlap with Al_2O_3 (113), the ferrite {220} and austenite {222} overlap, and the austenite {311} overlaps with Al_2O_3 (134). However, the austenite {200} and {220} peaks are distinct and can be used to follow the behavior of the austenite in the high-temperature region. As anticipated, there are also some minor shifts in the peak positions for the different grades due to the varying alloying levels (Table I).

Grades 2304, 2101, 2507, and 3207 were all measured *in-situ*, and during the heating, the amount of austenite was expected to decrease with increasing temperature by transformation to ferrite ($\gamma \rightarrow \alpha$) in the high-temperature region. Figure 3 shows the *in-situ* diffraction data for 2507 and 3207 as a function of temperature during heating to 1703 K (1430 °C) and cooling to 873 K (600 °C) at the same rate (4 K/min). It should be noted that the steel peaks shifted to lower scattering angles (as compared to Figure 2) due to thermal expansion. During heating, all grades showed the same behavior; *i.e.*, when increasing the temperature, the austenite peaks became weaker in intensity and ultimately disappeared, as seen for 2507 and 3207 in Figure 3. At the point of dissolution, the austenite peaks dropped at the same time, even though the stronger {220} was slightly clearer compared to {200}. For the 2507, it was also noted that the ferrite {200} faded and that a new {200} peak developed at ~1673 K (1400 °C); a new {220} peak was also developed from ~1573 K (1300 °C). During the temperature ramp down, the austenite peaks returned; this was noted to occur at a lower temperature compared to where the peaks disappeared (Figure 3). For 3207, it was also noted that three new peaks (hardly visible) appeared below 1073 K (800 °C) (between $2\theta =$

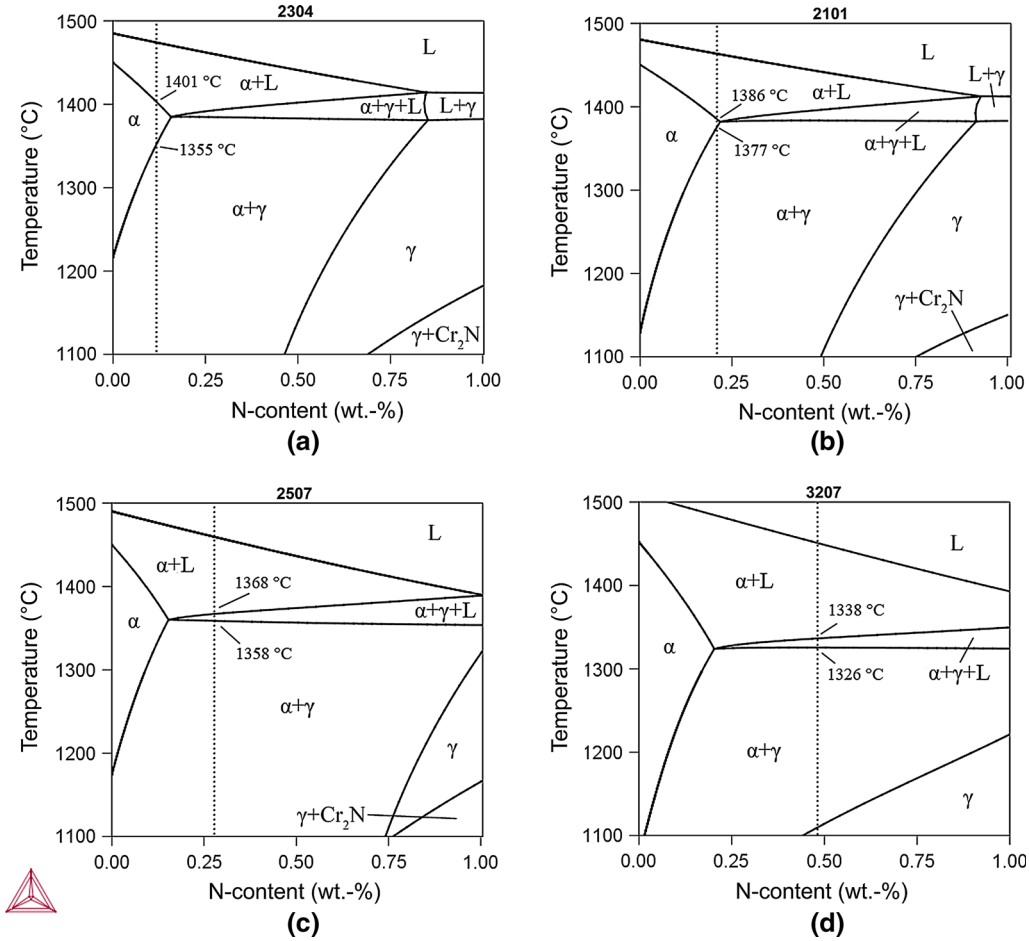

Fig. 1—Calculated isopleth sections for (*a*) 2304, (*b*) 2101, (*c*) 2507, and (*d*) 3207 with nitrogen contents up to 1 wt pct using the TCFE7 database.[15] The batch analysis nitrogen content is indicated by the dashed lines (the uncertainty of the analysis is at the ±0.01 level).

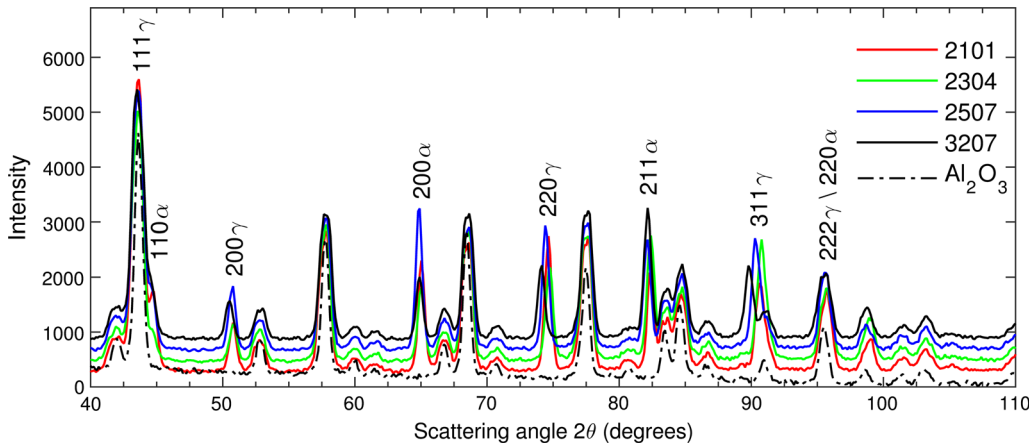

Fig. 2—Ambient temperature neutron diffraction patterns for grades 2101, 2304, 2507, and 3207 imposed on the Al_2O_3 pattern showing the overlaps with the sample holder. The ferrite {110} and austenite {111} both overlap with Al_2O_3 (113), and austenite {311} overlaps with Al_2O_3 (134). Austenite {200} and {220} were used to monitor the behavior of the austenite during progressive heating.

45 deg and 48 deg) corresponding to the σ-phase (212), (411), and (331) peaks.[16]

For a more accurate determination of the austenite dissolution temperatures, the intensities of the austenite {200} and {220} peaks were summed for each temperature, as shown in Figure 4. As expected, the dissolution occurred gradually with increasing temperature and complete dissolution was eventually observed in all grades. It is obvious that dissolution occurred first in the lean grades, at 1613 K (1340 °C) for 2304 and 1618 K (1345 °C) for 2101, and later in the more alloyed grades, at 1648 K (1375 °C) for 2507 and 1658 K (1385 °C) for

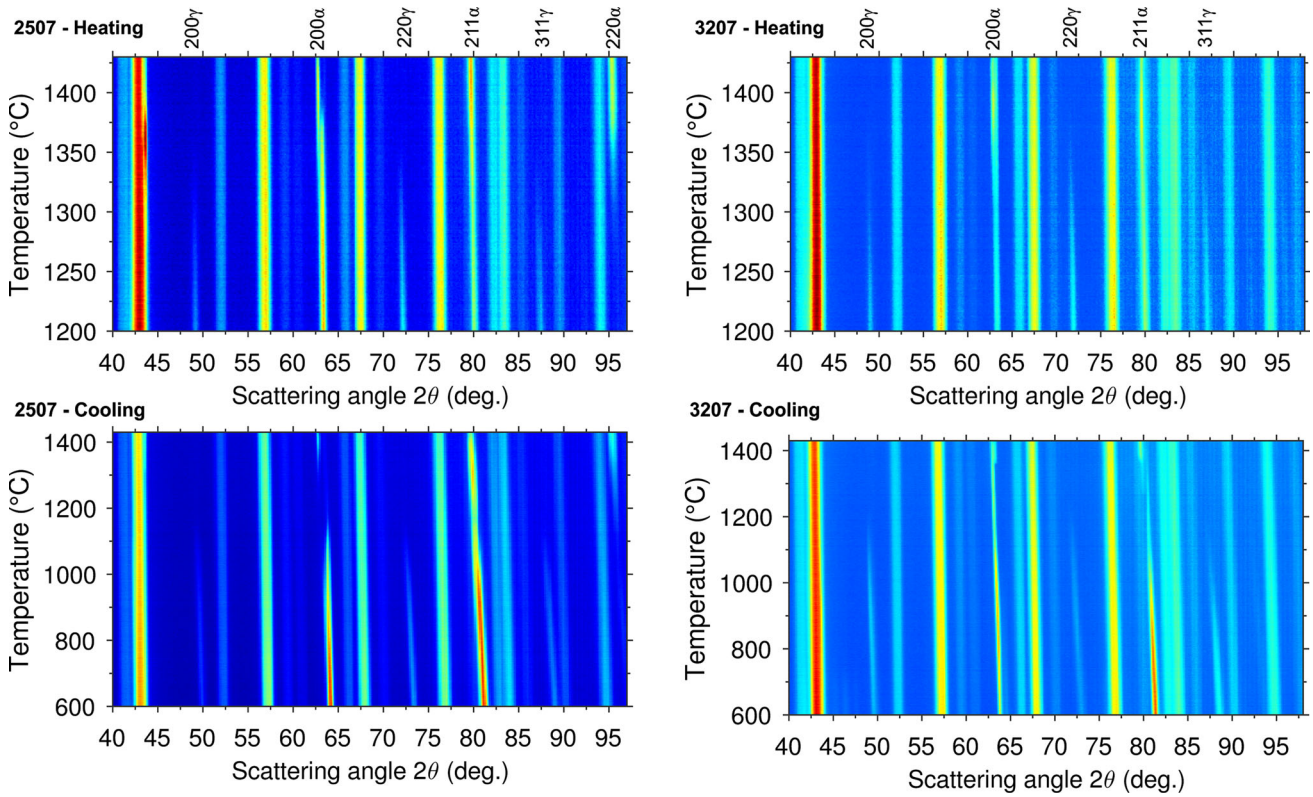

Fig. 3—*In-situ* neutron diffraction data as a function of temperature during progressive heating at 4 K/min from 1473 K to 1703 K (1200 °C to 1430 °C) followed by cooling from 1703 K to 873 K (1430 °C to 600 °C) at 4 K/min for 2507 and 3207.

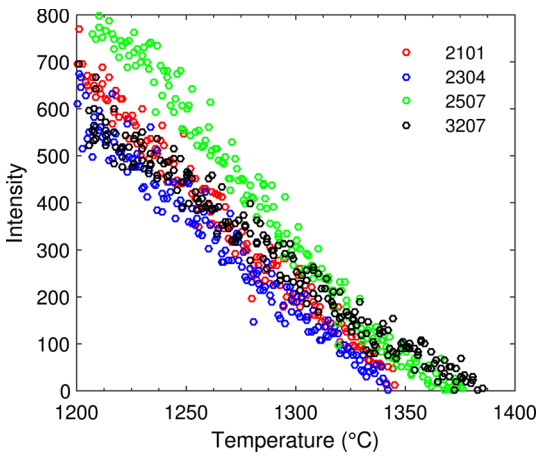

Fig. 4—Summed intensity of austenite peaks {200} and {220} as a function of temperature showing dissolution of the austenite phase in different grades.

3207. During cooling, the austenite started to form at approximately 1518 K (1245 °C) in 2304, 1538 K (1265 °C) in 2101, 1483 K (1210 °C) in 2507, and 1513 K (1240 °C) in 3207.

If the phase equilibria comprise a ferritic region, the material should not have started melting before the austenite was dissolved during heating. In the diffraction data, it would be expected that the scattering from the ferrite increases when the austenite is being dissolved and that any simultaneous intensity drop in the ferrite peaks does not occur until after dissolution of the austenite. However, the situation becomes complicated by the fact that all peaks are not visible due to overlaps and that the materials become textured during high-temperature exposure.

For the 2304 and 2101, the austenite was dissolved at 1613 K (1340 °C) and 1618 K (1345 °C). This was relatively low compared to the calculated melting temperatures (Figure 1) of 1678 K (1401 °C) and 1659 K (1386 °C), respectively. A drop in the ferrite peaks could not be seen up to 1648 K (1375 °C), and the solidus temperatures, thus, appeared to be higher. Therefore, 2304 and 2101 were concluded to be single-phase ferritic above their measured austenite dissolution temperatures.

For the 2507 and 3207, on the other hand, the measured austenite dissolution temperatures were higher than or closer to the calculated melting temperatures 1631 K (1358 °C) and 1599 K (1326 °C) (Figure 1). A detailed assessment of all peaks, therefore, is shown in Figures 5(a) and (b). In the case of 2507 (Figure 5(a)), three ferrite peaks are seen after the austenite was dissolved at 1648 K (1375 °C). Above that temperature, one part of the splitting {200} peak, the {211}, and the {220} all gain in intensity upon heating. The {200} and {211} then start dropping after reaching 1673 (1400 °C) and 1683 K (1410 °C), respectively. The {220}, however, still gains in intensity up to 1703 K (1430 °C) (the maximum temperature). The fact that some of the ferrite peaks decreased while others gained

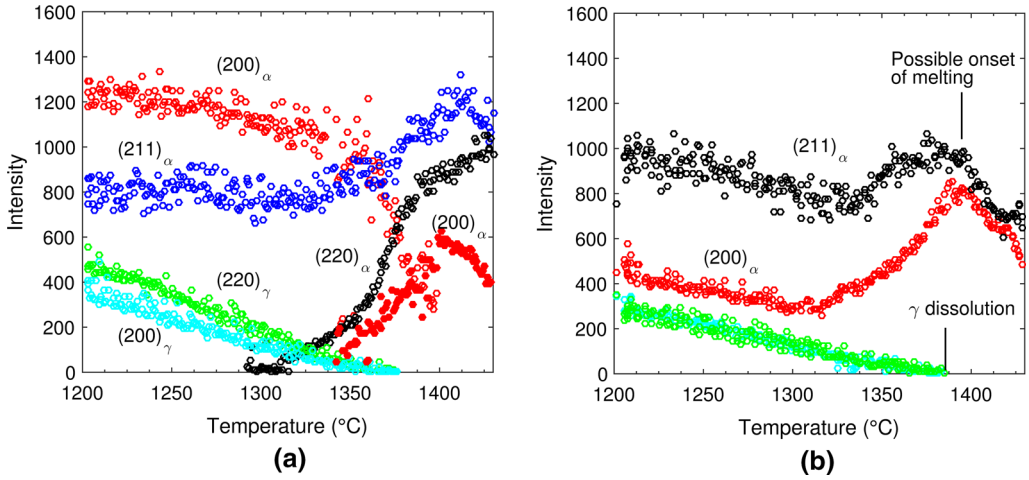

Fig. 5—Intensity of all nonoverlapping ferrite and austenite peaks as a function of temperature for (*a*) 2507 and (*b*) 3207.

in intensity would indicate grain growth rather that the formation of liquid. It is, thus, safe to conclude that the 2507 is single-phase ferritic from 1648 K (1375 °C) and up to a minimum of 1673 K (1400 °C).

In the case of 3207 (Figure 5(b)), the austenite is dissolved at 1658 K (1385 °C). There are two visible ferrite peaks, namely, {211} and {200}, that both increase in intensity during the later stages of austenite dissolution and for continued heating up to 1668 K (1395 °C). At that point, both ferrite peaks drop, which could indicate that the solidus temperature has been exceeded and that the liquid has started to form. It is, thus, indicated that the temperature interval over which the 3207 could be ferritic is limited to only ~10 K.

C. *Isothermal Heat Treatments and Microstructural Analysis*

Isothermal heat treatments were performed to confirm the *in-situ* observations of austenite dissolution, and the resulting microstructures after quenching were analyzed by EBSD to determine the distribution of austenite and the ferrite grain size. In the quenched microstructure, one must then distinguish between any undissolved austenite belonging to the as-received microstructure and the austenite that has formed upon quenching after the heat treatment. The undissolved austenite will be present in the form of lamellas (rounded in shape) that are elongated in the rolling direction, while the austenite that has formed upon quenching is present in the form of grain boundary allotriomorphs and Widmanstätten precipitates. However, if the material has become single phase during heat treatment, this would also be noticed from the change in shape and size of the ferrite grains.

For each grade, isothermal heat treatments were performed sequentially approaching the measured austenite dissolution temperature, and phase colored EBSD maps of the resulting microstructures are shown in Figure 6. It can be seen that the originally banded microstructure is gradually broken up with increasing temperature and that the austenite is ultimately dissolved in all grades concluded from the observation that only the austenite that has formed upon quenching is present. It is further seen that the temperatures for austenite dissolution in the isothermal heat treatments are in agreement with the austenite dissolution temperatures measured *in-situ*: 1603 to 1613 (1613) K for 2304, 1613 to 1623 (1618) K for 2101, 1643 to 1653 (1648) K for 2507, and 1658 to 1663 (1658) K for 3207.

From the *in-situ* measurements, it is clear that the structure was completely ferritic after dissolution of austenite for all grades, besides the 3207 where the measured ferritic range appeared narrow. In Figure 6, the existence of a fully ferritic structure is verified for three of the grades (2304, 2101, and 2507) by the change of the ferrite grain size after heat treatment at the highest temperature. It can be seen that dissolution of the austenite has resulted in unhindered ferrite grain growth. The 3207, on the other hand, behaves differently. The microstructure was completely free from the lamellar type austenite after heat treatment at 1663 K (1390 °C) (low amounts were still observed after heat treatment up to 1662 K). However, in contrast to the other grades, dissolution of austenite did not result in any appreciable ferrite grain growth, and the geometrically different austenite allotriomorphs in the same sample are apparent (Figure 6). This difference was further examined by looking at the austenite and ferrite crystallographic orientations. Figure 7 shows inverse pole figure (IPF) colored maps of the austenite in 3207 after quenching from 1658 K to 1663 K (1385 °C to 1390 °C), respectively. In the former, numerous austenite allotriomorphs that clearly are results of separate nucleation events are seen in the ferrite grain boundaries. It is known that solid-state formation of austenite allotriomorphs in ferrite grain boundaries can occur with a near Kurdjumov–Sachs (K–S) orientation relationship (OR)[17] ($\{111\}_\gamma \| \{110\}_\alpha$ and $\langle 1\bar{1}0\rangle_\gamma \| \langle 1\bar{1}1\rangle_\alpha$) toward one of the ferrite grains.[18–20] Such interfaces are observed for some of the grain boundary allotriomorphs in Figure 7(a) (boundaries that are in <10 deg proximity of the K–S OR are colored black). It can also be seen that the intragranular austenite exhibits K–S

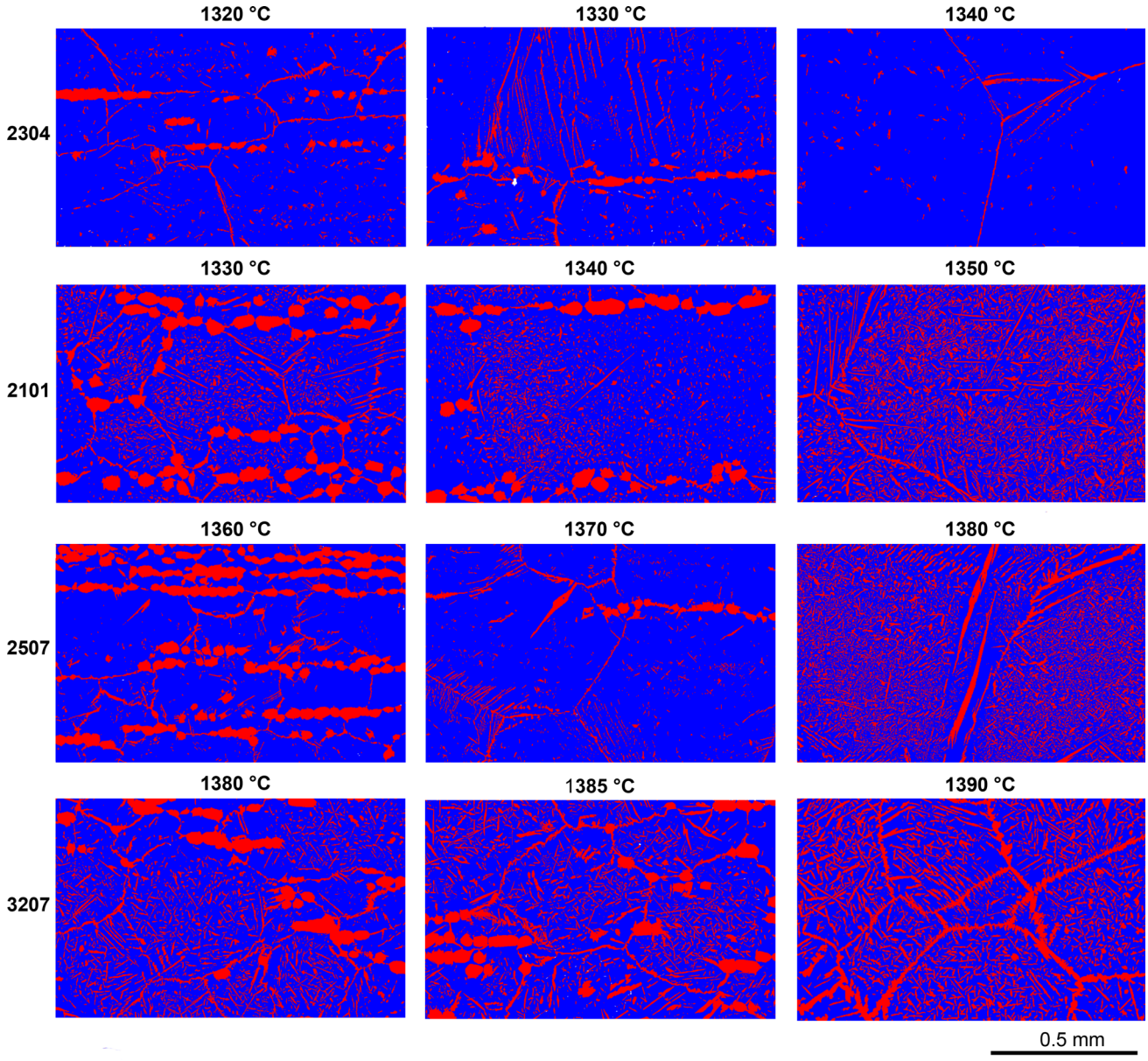

Fig. 6—Phase colored EBSD maps of as-quenched microstructures showing austenite (red) and ferrite (blue) for 2304, 2101, 2507, and 3207 after isothermal heat treatments for 0.5 h in proximity of the austenite dissolution temperature. The 2304, 2101, and 2507 are oriented with the horizontal rolling direction; the 3207 is oriented with the horizontal extrusion direction.

orientation, as also observed by Chen and Yang.[21] After quenching from 1663 K (1390 °C), the austenite allotriomorphs are noticeably coarser (Figure 7(b)) and no distinct K–S oriented boundaries are observed. The intragranular Widmanstätten austenite, on the other hand, still exhibits near K–S OR with the ferrite. In fact, the main part of the allotriomorphs in Figure 7(b) comprises only one single crystal of austenite, as indicated by the IPF coloring (this was also confirmed by construction of a pole figure). Thus, it appears that austenite allotriomorphs present after quenching the 3207 from 1658 K (1385 °C) have been formed by the solid-state reaction $\alpha \rightarrow \gamma$. The extension and different orientation of the allotriomorphs found after quenching from 1663 K (1390 °C) could instead indicate that the grain boundaries have been partially melted at this stage and that the austenite allotriomorphs have formed by the reaction $L + \alpha \rightarrow \gamma$, hence, through a different nucleation and growth mechanism. The narrow ferritic region indicated in the *in-situ* measurement, therefore, cannot be confirmed, and the solvus temperature appears to more likely be on the limit to the $\alpha + \gamma + L$ three-phase equilibria.

Regarding the change in the microstructure with temperature in Figure 6, it can be seen that the ferrite grain growth is, to some extent, hindered up to the point of austenite dissolution since the austenite is located in the grain boundaries. For the heat-treated 3207, it is noted that the grain size did not significantly change after dissolution of the austenite, which could be an

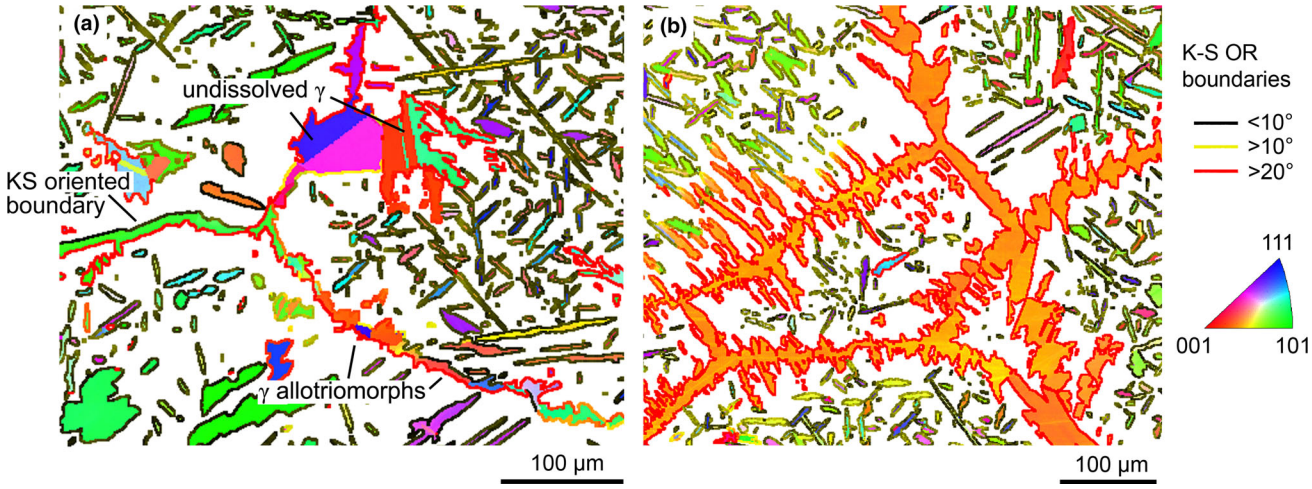

Fig. 7—IPF colored EBSD maps showing the orientation of austenite in 3207 after isothermal heat treatments at (*a*) 1658 K (1385 °C) and (*b*) 1663 K (1390 °C) and quenching. The phase boundaries are colored according to the deviation of K–S orientation with ferrite.

Table II. Nitrogen Levels in Wt Pct Measured by Combustion Analysis Before and After Exposure to the *In-Situ* and Isothermal Heat Treatments for the Different Grades

Grade	As-Received Condition	After *In-Situ* Experiment	Isothermal Heat Treatment at Temperature								
			1593 K (1320 °C)	1603 K (1330 °C)	1613 K (1340 °C)	1623 K (1350 °C)	1633 K (1360 °C)	1643 K (1370 °C)	1653 K (1380 °C)	1663 K (1390 °C)	1673 K (1400 °C)
2304	0.12	0.050	0.13	0.13	0.12	—	0.12	—	—	—	—
2101	0.22	0.077	—	0.22	0.22	0.22	0.22	—	0.22	—	—
2507	0.28	0.075	—	—	—	—	0.29	0.29	0.29	0.29	—
3207	0.48	0.180	—	—	—	—	—	0.46	0.46	0.48	0.47

effect of grain boundary pinning by liquid wetting of the grain boundaries. These results indicate that the high-temperature stability of the austenite and the width of the ferritic range will be beneficial factors for making the material less sensitive to high-temperature exposure. This is important in the HAZ of welds, where a fine grain size will enhance the austenite formation during cooling, which is needed to obtain the desired ferrite-austenite phase ratio.[8] An enlarged ferrite grain size will instead promote nonequilibrium nitride precipitation in the ferrite grain interior due to nitrogen supersaturation.[22] It is important to note that overalloying, particularly of nitrogen, could shift the solidification mode and potentially lead to problems with formation of gas porosity during solidification.[23]

D. *Analysis of the Postexperimental Nitrogen Content*

The nitrogen levels were measured after the different heat treatments, and the results are presented in Table II. All the grades had lost nitrogen after the *in-situ* experiments, while the nitrogen contents still remained at the levels of the as-received conditions after the isothermal heat treatments (*i.e.*, no losses occurred in that case). The extent of nitrogen desorption (Table II) further emphasizes the importance of using a method with a large analysis depth.

The mechanism for nitrogen desorption/adsorption has been explained to depend on the nitrogen partial pressure and the surface availability of atomistic nitrogen, which is disturbed by the surface-active elements sulfur and oxygen.[24,25] Therefore, it is not surprising that the samples heat treated in ambient atmosphere had lower susceptibility to nitrogen desorption than the samples exposed in the nitrogen and oxygen-free argon atmosphere.

Loss of nitrogen from the steel will influence the thermodynamic equilibria in the affected region. According to Figure 1, a nitrogen loss will shift the austenite stability to lower temperatures. No indications of nitrogen losses before dissolution of the austenite were seen in the diffraction data during heating. From the observation that the austenite precipitated at lower temperature during cooling in the *in-situ* experiment, it is reasonable to conclude that the nitrogen desorption mainly occurred in the ferritic state, since that is where the solubility of nitrogen is lowest and the diffusivity is highest. While still present in the microstructure, the austenite is expected to allocate most of the nitrogen and will also obstruct the diffusion path to the surface within the ferrite. This means that the austenite dissolution temperature could be underestimated if measured in the surface region, but not temperatures measured for the bulk (as also confirmed by the isothermal heat treatments in this case). It is important to note, however, that nitrogen desorption in the ferritic state will result in an overestimation of the solidus temperature, as seen when shifting the composition in the isopleths in Figure 1 to

lower nitrogen contents. In practical situations, nitrogen losses are unwanted and will lead to lowered pitting corrosion resistance of the HAZ in welds due to a reduced ability for austenite formation during subsequent cooling.[8,9]

E. *Comparison to Thermodynamic Calculations*

From the thermodynamic calculations, only the grade 2304 was predicted to have a high-temperature single-phase ferritic region calculated to lie between 1628 K (1355 °C) and 1674 K (1401 °C). The calculations for the 2101 were more uncertain showing only a narrow ferritic region between 1650 K (1377 °C) and 1659 K (1386 °C). The measured ferrite solvus temperatures for these grades were 1613 K (1340 °C) for 2304 and 1618 K (1345 °C) for 2101.The 2507 and 3207 were both outside the ferritic range in the calculations, however, with the austenite stable up to 1641 K (1368 °C) in 2507 and 1611 K (1338 °C) in 3207. The measured experimental values of the austenite stability were 1648 K (1375 °C) for 2507 and 1658 K (1385 °C) for the 3207. There is, thus, a notable discrepancy between the thermodynamic calculations and the experimental results, and the high-temperature phase equilibria are not correctly reproduced for the higher alloyed grades 2507 and 3207.

From the calculated isopleths in Figure 1, it appears that the nitrogen solubility in ferrite could be underestimated, or that the solubility in austenite could be overestimated, and that the ferrite single-phase field should be extended more in its upper nitrogen end. However, while the measured austenite dissolution temperatures suggest that the ferritization temperature is underestimated for 3207, the temperature is overestimated for 2101 and 2304. The influence of nitrogen solubility, therefore, does not appear unambiguous, and in the present eight-component system, there are several binary and ternary subsystems that could influence the results. A thorough revision of the related subsystems is needed, where the present data could be used as control points to give insight in the database precision in the high-temperature region for duplex stainless steels.

The Thermo-Calc software has been applied previously as a tool for design of duplex stainless steel grades, as illustrated by the patent for SAF 2507,[26] where calculations with the steel database TCFE99 were used to optimize the composition so that an equal pitting resistance equivalence was obtained in both ferrite and austenite. The present results indicate that the high-temperature microstructural stability could be influenced by the design of the ferritic range—a task that would then require a thermodynamic database with high precision also in the high-temperature region.

IV. CONCLUSIONS

The high-temperature phase equilibria were investigated for duplex stainless steels 2304, 2101, 2507, and 3207 by observing the behavior of the constituent phases ferrite and austenite *in-situ* using neutron scattering during progressive heating at a rate of 4 K/min. The measured austenite dissolution temperatures were 1613 K (1340 °C) for 2304, 1618 K (1345 °C) for 2101, 1648 K (1375 °C) for 2507, and 1658 K (1385 °C) for 3207, which was also confirmed by isothermal heat treatments. Three of the alloys (2304, 2101, and 2507) clearly possess a ferritic single-phase region below solidus. It is clear that this ferritic region becomes narrower with increased levels of alloying; in fact, for the highest alloyed grade 3207, the ferritic region is close to zero.

ACKNOWLEDGMENTS

This work was funded by the Swedish government agency for innovation Vinnova (Grant No. 2013-03258) and by the project partners AB Sandvik Materials Technology, Outokumpu Stainless AB, Norwegian Material Center of Expertise AS (NOMAC), Thermo-Calc Software AB, and KTH Royal Institute of Technology. The authors gratefully acknowledge the Australian Nuclear Science and Technology Organization for the beam time (proposal 4215). We are also grateful to the Axel Hultgrens Stiftelse and the Hugo Carlssons Stiftelse for financial support. Further, we acknowledge Dr. Ryan Cottam (Swinburne University of Technology) for assistance during the measurements and thank Drs. Fredrik Lindberg and David Lindell (Swerea KIMAB) for the valuable discussions. We also acknowledge Professors Rachel Pettersson (Jernkontoret) and Annika Borgenstam (KTH) for comments on the manuscript.

REFERENCES

1. J.-O. Nilsson: *Mater. Sci. Technol.*, 1992, vol. 8, pp. 685–700.
2. S. Hertzman and J. Charles: *Rev. Métall.*, 2012, vol. 108, pp. 413–25.
3. R. Lillbacka, G. Chai, M. Ekh, P. Liu, E. Johnson, and K. Runesson: *Acta Mater.*, 2007, vol. 55, pp. 5359–68.
4. S. Harjo, Y. Tomota, P. Lukas, D. Neov, M. Vrana, P. Mikula, and M Ono: *Acta Mater.*, 2001, vol. 49, pp. 2471–79.
5. R.F.A. Jargelius-Pettersson: *Corros. Sci.*, 1999, vol. 41, pp. 1639–64.
6. S.J. Pawel, E.E. Stansbury, and C.D. Lundin: *Corrosion*, 1989, vol. 45, pp. 125–33.
7. H. Okamoto, in *Proceedings of the Conference on Applied Stainless Steels '92,* 1992, pp. 360–69.
8. S. Hertzman, B. Brolund, and P. Ferreira: *Metall. Mater. Trans. A*, 1997, vol. 28A, pp. 277–85.
9. S. Hertzman, R.J. Pettersson, R. Blom, E. Kivineva, and J. Eriksson: *ISIJ Int.*, 1996, vol. 36, pp. 968–76.
10. D.J. Kotecki, T.A. Siewert, *WRC-1992 Constitution Diagram for Stainless Steel Weld Metals: A Modification of the WRC-1988 Diagram,* AWS Annual Meeting, 1992, pp. 171–78.
11. A.J. Ramirez, J.C. Lippold, and S.D Brandi: *Metall. Mater. Trans. A*, 2003, vol. 34A, pp. 1575–97.
12. T.A. Palmer, J.W. Elmer, and S.S. Babu: *Mater. Sci. Eng. A*, 2004, vol. 374, pp. 307–21.
13. A.J. Studer, M.E. Hagen, and T.J. Noakes: *Phys. B Condens. Matter*, 2006, vols. 385–386, pp. 1013–15.
14. J.O. Andersson, T. Helander, L. Höglund, P. Shi, and B. Sundman: *Calphad*, 2002, vol. 26, pp. 273–312.
15. Thermo-Calc Software AB, TCFE7 Steels/Fe-alloys database version 7.

16. J.W. Elmer, T.A. Palmer, and E.D. Specht: *Metall. Mater. Trans. A*, 2007, vol. 38A, pp. 464–75.
17. G. Kurdjumov and G. Sachs: *Z. Phys.*, 1930, vol. 64, pp. 325–43.
18. N. Suutala, T. Takalo, and T. Moisio: *Metall. Trans. A*, 1979, vol. 10A, pp. 1183–90.
19. C.H. Shek, C. Dong, J.K.L. Lai, and K.W. Wong: *Metall. Mater. Trans. A*, 2000, vol. 31A, pp. 15–19.
20. S. Hertzman: *ISIJ Int.*, 2001, vol. 41, pp. 580–89.
21. T.H. Chen and J.R. Yang: *Mater. Sci. Eng. A*, 2002, vol. 338, pp. 166–81.
22. N. Pettersson, R.F.A. Pettersson, and S. Wessman: *Metall. Mater. Trans. A*, 2015, vol. 46A, pp. 1062–72.
23. Y.-H. Park and Z.-H. Lee: *Mater. Sci. Eng. A*, 2001, vol. 297, pp. 78–84.
24. J.D. Katz and T.B. King: *Metall. Trans. B*, 1989, vol. 20B, pp. 175–85.
25. T.A. Palmer and T. Debroy: *Weld. Res.*, 1996, vol. 75, pp. 197–207.
26. P. Hagenfeldt, S. Bernhardsson, S. Lagerberg, *High Nitrogen Containing Duplex Stainless Steel Having High Corrosion Resistance and Good Structure Stability,* 1988.